

## High resolution image in bone biology II. Review of the literature

Jorge Cano <sup>1</sup>, Julián Campo <sup>1</sup>, Juan José Vaquero <sup>2</sup>, Jose María Martínez-González <sup>3</sup>, Antonio Bascones <sup>4</sup>

(1) Lecturer, School of Dentistry, UCM

(2) Researcher, Image Lab, Medicine and Experimental Surgery, Gregorio Marañón General University Hospital, Madrid

(3) Senior lecturer, School of Dentistry, UCM

(4) Professor, School of Dentistry, UCM

### Correspondence:

Dr. Jorge Cano Sánchez

Departamento de Medicina y Cirugía Bucofacial

Facultad de Odontología (UCM).

Avda Complutense s/n 28040 Madrid. Spain

Email: jo.cano@wanadoo.es

Received: 23-02-2007

Accepted: 17-06-2007

### Indexed in:

-Index Medicus / MEDLINE / PubMed  
-EMBASE, Excerpta Medica  
-SCOPUS  
-Indice Médico Español  
-IBCS

Cano J, Campo J, Vaquero JJ, Martínez-González JM, Bascones A. High resolution image in bone biology II. Review of the literature. Med Oral Patol Oral Cir Bucal. 2008 Jan1;13(1):E31-5.

© Medicina Oral S. L. C.I.F. B 96689336 - ISSN 1698-6946

<http://www.medicinaoral.com/medoralfree01/v13i1/medoralv13i1p31.pdf>

### Abstract

Bone microstructure has usually been assessed by obtaining samples invasively and analyzing them with conventional histomorphometric methods. Improvements in high-resolution image acquisition systems have enabled non-invasive assessment of bone morphology and a more precise 3-D evaluation by means of “virtual biopsies”, permitting bone assessment in regeneration or remodeling processes. Among other applications, this imaging technique can be used for the ultrastructural analysis of bone and for studies of regeneration techniques, biomechanics in bone physiotherapy, and periimplant bone healing. This review describes the different applications of high-resolution imaging techniques in bone biology and the morphometric results obtained with these images in mechanobiology in general and maxillary bone in particular.

**Key words:** High-resolution image, bone biology, virtual biopsy.

### Introduction

The interaction between mechanical signals and biological processes in cells and tissue is studied in mechanobiology. Mechanical load may influence cell proliferation, differentiation and metabolism and therefore have a crucial role in live tissue growth, adaptation, regeneration and bioengineering. Mechanobiology combines experimental biological techniques (in vitro and in vivo models) and computerized techniques (mathematical and computer models) to create interactions between mechanics and biology.

Van der Meulen described skeletal mechanobiology as “the science that studies the mechanical forces that modulate morphological and structural fitness of skeletal tissue, i.e., bone, cartilage, ligament and tendon” (1). Three developments have led to major advances in bone mechanobiology in recent years: a) computer models of structures, allowing analysis of the effects of physical

force on the complex bone geometry; b) molecular biology, permitting detection of gene expression and protein synthesis after applying different mechanical forces, and c) novel imaging technology, revealing the micro- and nanostructural characteristics of tissue (1).

Real high-resolution images can serve as a source of data for generating Finite Element (FE) computer programs, providing a more accurate simulation of different biomechanical load situations compared with conventional FE. The study of bone biomechanics is relevant to bone physiopathology (e.g., osteoporotic state or fracture risk), bone-biomaterial interface (e.g., periimplant healing), and bone regeneration (e.g., distraction histogenesis and fracture healing). Unlike traditional biomechanical methods, computerized micro-FE models ( $\mu$ FEs) can simulate the different biomechanical properties of bone (compression, tension, shearing or fatigue) (2) and do not require the destruction of samples.

$\mu$ FE models can be developed from the image by the voxel conversion technique, using cubic elements (hexahedrons) or tetrahedrons. Around  $10^5$ - $10^6$  cubic elements are usually required to reconstruct  $1 \text{ cm}^3$  of trabecular bone (3), and it is considered that the size of each element should not exceed by  $>25\%$  the average thickness of a trabecula (4). The tetrahedron system yields more reliable results in the FE study, since it represents a closer approximation to trabecular connections (5). Advances in computers have enabled construction of  $\mu$ FEs of the proximal area of human femur that use 100 million elements to study the distribution of deformations. However, the computer memory required to create  $\mu$ FE of a complete bone remains excessive (3).

This review describes applications of bone mechanobiology studies to both long and maxillary bones and explores the usefulness of high-resolution images in maxillary regeneration and osseointegration techniques.

### General bone mechanobiology with high-resolution images

Among studies of *biomechanics in bone physiopathology*, Takada et al. (6) used micro-computed tomography ( $\mu$ CT) and  $\mu$ FE to assess the distribution of stress at the mandibular angle with presence and absence of impacted third molars. They observed that the retromolar area had vertical trabeculae above the mandibular canal and horizontal lingual-buccal trabeculae below it. In mandibles with impacted third molar, stress was concentrated around the root apex of this tooth, spreading to the mandibular base, whereas stress was distributed along the canal throughout the mandible in their absence. However, the presence of impacted third molars at mandibular angle had no effect on bone microstructure parameters, i.e., bone volume/tissue volume (BV/TV), trabecular number (Tb.N), degree of anisotropy (DA), or structure model index (SMI).

McNamara et al. (7) developed a solid model from four trabeculae of rat tibia and femur using  $\mu$ CT and  $\mu$ FE analysis, allowing them to observe the reaction to loads on a model with a real morphology, including active resorption lacunae. This computer model showed that a stress load of  $3000 \mu\epsilon$  applied on each trabecula had a heterogeneous distribution, with deformation measurements above  $4000 \mu\epsilon$  (upper limit of physiological range) in  $\geq 30\%$  of trabeculae. High stress was observed at the base of resorption lacunae, producing greater osteoclastic activity than initially estimated for the renewal of old or damaged bone. It also prevented a homogeneous distribution of the load throughout the trabeculae, which was achieved in absence of these lacunae. Stress levels of 144 MPa were observed in some areas, with a deformation of up to  $64300 \mu\epsilon$ . Given that trabecular (cancellous) bone shows fatigue failure at 100-140 MPa after 100,000 cycles and even deformation of 5000-10,000  $\mu\epsilon$  after only 1,000-100,000 cycles (8), trabecular fracture risk would be increased by

loads on these areas of resorption. It is not known why resorption of this basic multicellular unit (BMU) stops at a given point, although it may be when lower stress is detected or when a layer of new more resistant laminar bone is encountered.

There are some limitations to the creation of FE-based models. Tissue stress and deformation depend on the properties of the material (5). FE studies have established different elasticities (Young's modulus) for cortical and trabecular bone (9). However, no data have been published on the biomechanical properties of immature bone (reticular and parallel fibers) interlaced with laminar bone during remodeling and regeneration processes (10). Hence, finite elements present mechanical properties that are close to real bone conditions, but they have yet to include all of the data needed to completely simulate bone structure.

The drawback of not being able to distinguish between different degrees of bone mineralization is being overcome by means of synchrotron radiation images (11). With an isotropic voxel resolution of  $4 \mu\text{m}$ , 3-4 hrs are required to scan a biopsy of human iliac crest. Because the radiation is monochromatic, distinct mineral concentrations in the bone appear as different gray level intensities, allowing discrimination between mature bone (darker laminar areas) and immature bone (lighter areas with reticular/parallel fibers) (11). This imaging system opens up the way for  $\mu$ FE studies of different specific concentrations of mineralized bone.

Because the sample does not need to be destroyed,  $\mu$ CT imaging is a useful tool to assess bone architecture subject to static or dynamic loads, examining stress propagation, the start of structural failure and accumulation of damage. Müller et al. (12) developed a compression chamber for  $\mu$ CT study at the moment a load was applied on trabecular bone samples. The procedure allowed real-time observations of local failure patterns as a function of different loads. Structural modifications of the trabeculae were observed, and animation software was used for dynamic observation of the deformations. In structures with a rod-like pattern (as in osteoporotic state), an initial flexion was followed by collapse of the overloaded trabeculae. In plate-like structures, however, flexion was not observed when the same amount of load was applied, and the trabeculae collapsed later (vs. rod-like structures) and spontaneously, with no previous flexion.

The same research group (13) used synchrotron radiation  $\mu$ CT (SR $\mu$ CT) in a system of dynamic trabecular bone compression, observing that microcracks started with a 1% deformation rate and spread when this rate reached 2%. All microcracks were quantified by means of a specific algorithm and were more frequently observed in rod-like or plate-like trabeculae that had perforations. Despite the failure produced by these microfractures, ligamentous structures (organic matrix) maintained the morphology of the trabecular network. Fractures caused longitudinal

delamination of trabeculae. This system allowed quantification of the column and thickness of fissures and the separation between them. 3-D assessment of microdefects appears to discredit some 2-D-based classifications. Thus, a 2-D-evaluated microcrack is seen to be a microfracture in 3-D and diffuse microdamage is identified as a microcrack in 3-D (Fig. 1).

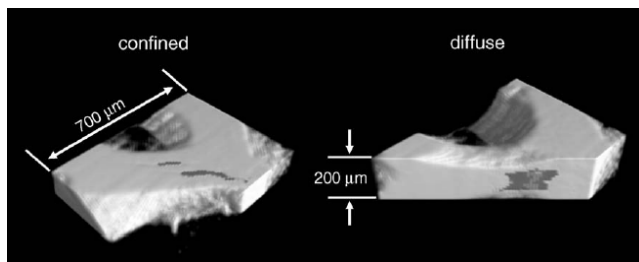


**Fig. 1.** 3-D image by SR $\mu$ CT (spatial resolution of 7 $\mu$ m). The same microcrack is observed from different angles. The same microcrack would be classified as a microcrack based on the image on the left but as diffuse microdamage based on the 3-D image. Published by permission of Professor Müller.

$\mu$ CT images have also been used for the study of *periimplant bone healing*. Very few studies have used  $\mu$ CT or SR $\mu$ CT (14). Gabet et al. (15) used 15- $\mu$ m resolution  $\mu$ CT to observe the healing of implants placed in metaphysis of osteoporotic rats (i.e., with low-density bone). This resolution enabled volumetric assessment of Bone Implant Contact (BIC) by evaluating voxels in contact with the implant. A significant correlation was observed between morphometric values and biomechanical parameters, demonstrating that morphometry based on high-resolution images is an adequate tool to assess the biomechanical properties of the bone-implant interface.

Experimental studies have also been performed with this type of image to observe biomechanical properties of the interface between bone and osteoconductor materials (e.g., polymers) (16). Different structures can be distinguished on tomographic images by using computer phase identification techniques, revealing the morphology, distortion and matrix surface properties. The connection between native and newly formed bone can also be observed. Regenerated bone within the matrix can be extracted “virtually”, predicting Young’s modulus for this new bone.

*Regenerating bone* has also been assessed in a non-invasive manner on high-resolution images. Rat femurs were used to study the biomechanics of fracture callus by means of  $\mu$ CT and  $\mu$ FE after 3-4 weeks healing (17). A Young’s modulus (E) value of 50 MPa was assigned for soft tissue, 5000 MPa for less mineralized bone, and 15000 MPa for highly mineralized bone, applying a Poisson coefficient ( $\nu$ ) of 0.3. Unlike conventional tests, this technique offers

flexion and torsion simulations in various spatial planes, which is a major advantage in cases of asymmetrical fracture callus. An improved prediction of callus rigidity was also obtained with this approach than with other radiographic methods, e.g., callus area or Bone Mineral Density (BMD).

### Assessment of maxillary bones with high-resolution images

High resolution imaging techniques are being used to study the maxillofacial skeleton for various purposes: a) to examine bone microstructure at different anatomic sites (18, 19); b) to evaluate the bone-implant interface during osseointegration (14); c) to study bone remodeling around teeth subject to orthodontic loading (20); d) to assess regenerating bone (20); and e) to evaluate the response of bone to biomaterials (21).

Because of the anisotropic nature of bone, attempts have been made to relate data obtained from 2-D images (e.g., conventional X-ray or histological images) to data from high-resolution 3-D images acquired by  $\mu$ CT or magnetic resonance imaging ( $\mu$ MRI). A grayscale can be used in a 2-D radiological image to determine the bone area of a sample. When a 3-D image is used, the BV/TV ratio is the best variable for establishing bone density. These two variables were found to be correlated with each other and with the biomechanical resistance of trabecular bone in pig mandible (18).

Chöel et al. (19) used  $\mu$ MRI for a *microstructural study* of the mandible of elderly human corpses. They studied apparent 2-D parameters (sections of >600 $\mu$ m) and found higher B.Ar/T.Ar, Tb.Th, and DA values in male than in female samples. They reported the high anisotropy of mandibular trabecular bone and its orientation perpendicular to the axis of the teeth, when these were present. The highest degree of anisotropy was in the incisal region, the area least affected by masticatory load.

A  $\mu$ CT study of human mandibles (22) found higher BV/TV, Tb.Th and Tb.N values and lower BS/BV, trabeculae separation (Tb.Sp), and SMI values in alveolar versus basal bone. Alveolar bone showed wider, plate-like trabeculae. The most porous trabecular pattern was in basal bone below the mandibular canal, which appears to be subject to lower masticatory loads.

Conventional CT Hounsfield values in human mandibles were compared with morphometric, densitometric, and biomechanical values obtained by means of  $\mu$ CT, Dual-Energy X-ray Absorptiometry (DEXA), and compression test, aiming to optimize the pre-operative assessment of bone quality proposed by de Letholm and Zarb (23). The conventional method proved valid for mandible samples with thin cortex but not for those with thick cortex, which appears to add errors to the image, increasing the trabecular bone density found by photon scattering. Therefore, quality classifications based on Hounsfield values should

be applied with caution in the clinical setting, since they are only valid when there is trabecular bone alone or with a thin cortex. With the  $\mu$ CT method, a BV/TV range of 11-73% was observed (24).

The trabecular bone of the mandibular condyle was shown to have an appropriate architecture for supporting the compression and tension loads generated by TMJ.  $\mu$ CT and  $\mu$ FE studies revealed a more rigid structure (higher Young's modulus) on the transversal (rod-like trabeculae) versus vertical (plate-like trabeculae) plane that showed a negative correlation with bone volume. Transversal trabeculae appeared to compensate for their lack of bone volume with a higher mineralization because they have a lower load rate and remodeling index and, consequently, a higher rigidity. Rigidity ranges obtained for mandibular trabecular bone were similar to those obtained (5-20 GPa) with conventional biomechanical or nanoindentation methods (4).

$\mu$ CT has also been used to observe alveolar bone architecture in mandible of growing rats after applying different mastication models. The use of an apparatus to generate open bite was seen to inhibit vertical growth and increase the thickness of mandibular cortex, possibly due to the constant increase in tension in the masseters, but no effects on trabecular architecture were observed. A group fed with a soft diet showed a reduction in mineral density, bone volume, and trabecular thickness (25).

Dental *implant osseointegration* involves a continuous remodeling process that depends on the biomechanical loads applied to the prosthesis-implant-bone complex. The biomechanical properties of the bone are governed by both its mineral content and its microarchitecture (26). Conventional histological images,  $\mu$ CT, and SR $\mu$ CT have been compared in the study of the bone-implant interface in mandibular bone. Bernhardt et al. (14) studied periimplant healing in dog mandibles at one month after placement of implants with different surface treatments (anodic oxidation, collagen partially integrated in the oxide layer, RGD-peptide immobilization, hydroxyapatite coating, and mineralized collagen coating). There were no significant differences in bone density values between conventional histology and SR $\mu$ CT imaging methods but the bone area was overestimated by  $\mu$ CT. Beam hardening errors are increased because of the broad energy spectrum produced by  $\mu$ CT and the high energy absorption of titanium, leading to observations of an apparent (not real) increase in absorption around the implant. At present, this effect can be corrected by an interactive beam hardening correction approach (27).

Alveolar bone response to *orthodontic loading* has been investigated. Verna et al. (28) observed the presence of microcracks in minipig mandible after applying orthodontic loads to the teeth. SR $\mu$ CT revealed a more irregular surface, with more microcracks in the lamina dura of the area under compression than in that subject to tension.

A pattern of linear microcracks was observed in the compression area, whereas a diffuse microdamage pattern was mainly found in the tension area. The periodontal ligament was thickened in the area to which the load was directed. The bone binding to the ligament was less mineralized, indicating its active remodeling due to a mechanical cause. These images revealed the periodontal vessels and fibers penetrating the alveolar bone and distinguished its different degrees of mineralization.

*Guided tissue regeneration* has usually been evaluated by means of bone histology and histomorphology. This conventional approach was compared with  $\mu$ CT imaging in rabbits (21). Morphological variables obtained with the two techniques showed a highly significant correlation ( $r^2$  0.72), with a difference in results of 16%. However, the  $\mu$ CT technique did not accurately detect osteoid, leading to an underestimation of bone volume. This type of image was also been used to assess periodontal regenerative therapy with heterologous materials (29), studying human samples with teeth at 15  $\mu\text{m}^3$  voxel resolution and 20-hr scan time.

$\mu$ CT was used to clinically evaluate bone regeneration in maxillary sinus after incorporation of alloplastic material and platelet rich plasma (PRP) (30). A 4-hr scan was required for a voxel size of 15x15x15  $\mu\text{m}^3$ . Different thresholds were employed to differentiate between graft particles and regenerated bone. The BV/TV values obtained by histomorphometry were 30% higher than those obtained with  $\mu$ CT. There were also differences in Tb.N, Tb.Th, and Tb.Sp findings between these methods. The same authors acknowledged some difficulty in determining the threshold to differentiate alloplastic material particles from newly formed bone, which was exacerbated by the small number of samples (n= 3) and the variability among them.

## Conclusions

The utilization of images acquired with  $\mu$ CT support subsequent simulation studies with finite elements or real-time load application investigations in a more precise way compared with conventional finite elements.

The new SR $\mu$ CT system yields similar resolutions to those obtained with histological samples. High-resolution images enable a more precise assessment in three dimensions, avoiding laborious sample processing and opening the way to in vivo morphometric assessments of bone tissue and the biomaterial-bone interface.

## References

1. Van der Meulen MC, Huiskes R. Why mechanobiology. A survey article. *J Biomech.* 2002 Apr;35(4):401-14.
2. Odgaard A. Three-dimensional methods for quantification of cancellous bone architecture. *Bone.* 1997 Apr;20(4):315-28.
3. Van Rietbergen B. Micro-FE analyses of bone: state of the art. En: Majumbar S, Bay BK, eds. *Noninvasive assessment of trabecular bone architecture and the competence of bone.* New York: Kluwer academic-Plenum Publishers; 2001 .p. 21-30.
4. Van Eijden TM, Van Ruijven LJ, Giesen EB. Bone tissue stiffness in

- the mandibular condyle is dependent on the direction and density of the cancellous structure. *Calcif Tissue Int.* 2004 Dec;75(6):502-8.
5. Ulrich D, Rietbergen B, Laib A, Riegsegger P. Mechanical analysis of bone and its microarchitecture based on in vivo voxel images. *Technol Health Care.* 1998 Dec;6(5-6):421-7.
  6. Takada H, Abe S, Tamatsu Y, Mitarashi S, Saka H, Ide Y. Three-dimensional bone microstructures of the mandibular angle using micro-CT and finite element analysis: relationship between partially impacted mandibular third molars and angle fractures. *Dent Traumatol.* 2006 Feb;22(1):18-24.
  7. McNamara LM, Van der Linden JC, Weinans H, Prendergast PJ. Stress-concentrating effect of resorption lacunae in trabecular bone. *J Biomech.* 2006;39(4):734-41.
  8. Carter DR, Caler WE, Spengler DM, Frankel VH. Fatigue behavior of adult cortical bone: the influence of mean strain and strain range. *Acta Orthop Scand.* 1981 Oct;52(5):481-90.
  9. Nicholson PH, Cheng XG, Lowet G, Boonen S, Davie MW, Dequeker J, et al. Structural and material mechanical properties of human vertebral cancellous bone. *Med Eng Phys.* 1997 Dec;19(8):729-37.
  10. Cano J, Campo J, Gonzalo JC, Moreno LA, Bascones A. Muestras de hueso sin descalcificar. Descripción de técnica y utilidad basada en la literatura. *Med Oral Patol Oral Cir Bucal* 2005; 10 Suppl 1:E74-E87.
  11. Borah B, Dufresne TE, Ritman EL, Jorgensen SM, Liu S, Chmielewski PA, et al. Long-term risedronate treatment normalizes mineralization and continues to preserve trabecular architecture: sequential triple biopsy studies with micro-computed tomography. *Bone.* 2006 Aug;39(2):345-52.
  12. Müller R, Gerber SC, Hayes WC. Micro-compression: a novel technique for the nondestructive assessment of local bone failure. *Technol Health Care.* 1998 Dec;6(5-6):433-44.
  13. Thurner PJ, Wyss P, Voide R, Stauber M, Stampanoni M, Sennhauser U, et al. Time-lapsed investigation of three-dimensional failure and damage accumulation in trabecular bone using synchrotron light. *Bone.* 2006 Aug;39(2):289-99.
  14. Bernhardt R, Scharnweber D, Müller B, Thurner P, Schliephake H, Wyss P, et al. Comparison of microfocus- and synchrotron X-ray tomography for the analysis of osteointegration around Ti6Al4V implants. *Eur Cell Mater.* 2004 Jun 30;7:42-51.
  15. Gabet Y, Müller R, Levy J, Dimarchi R, Chorev M, Bab I, et al. Parathyroid hormone 1-34 enhances titanium implant anchorage in low-density trabecular bone: a correlative micro-computed tomographic and biomechanical analysis. *Bone.* 2006 Aug;39(2):276-82.
  16. Jones AC, Sakellariou A, Limaye A, Arns CH, Senden TJ, Sawkins T, et al. Investigation of microstructural features in regenerating bone using micro computed tomography. *J Mater Sci Mater Med.* 2004 Apr;15(4):529-32.
  17. Shefelbine SJ, Simon U, Claes L, Gold A, Gabet Y, Bab I, et al. Prediction of fracture callus mechanical properties using micro-CT images and voxel-based finite element analysis. *Bone.* 2005 Mar;36(3):480-8.
  18. Huh KH, Yi WJ, Jeon IS, Heo MS, Lee SS, Choi SC, et al. Relationship between two-dimensional and three-dimensional bone architecture in predicting the mechanical strength of the pig mandible. *Oral Surg Oral Med Oral Pathol Oral Radiol Endod.* 2006 Mar;101(3):363-73.
  19. Choël L, Last D, Duboeuf F, Seurin MJ, Lissac M, Briguet A, et al. Trabecular alveolar bone microarchitecture in the human mandible using high resolution magnetic resonance imaging. *Dentomaxillofac Radiol.* 2004 May;33(3):177-82.
  20. Dalstra M, Verna C, Cacciafesta V, Andreassen TT, Melsen B. Micro-computed tomography to evaluate bone remodelling and mineralization . In: Majumbar S, Bay BK, eds. *Noninvasive assessment of trabecular bone architecture and the competence of bone.* New York: Kluwer academic-Plenum Publishers; 2001 .p. 9-19.
  21. Maréchal M, Luyten F, Nijs J, Postnov A, Schepers E, Van Steenberghe D. Histomorphometry and micro-computed tomography of bone augmentation under a titanium membrane. *Clin Oral Implants Res.* 2005 Dec;16(6):708-14.
  22. Moon HS, Won YY, Kim KD, Ruprecht A, Kim HJ, Kook HK, et al. The three-dimensional microstructure of the trabecular bone in the mandible. *Surg Radiol Anat.* 2004 Dec;26(6):466-73.
  23. Lekholm U, Zarb GA. Patient selection and preparation. In: Brånemark PI, Zarb GA, Albrektsson T, eds. *Tissue-integrated prostheses: osseointegration in clinical dentistry.* Chicago: Quintessence; 1985. p. 199-209.
  24. Stoppie N, Pattijn V, Van Cleynenbreugel T, Wevers M, Vander Sloten J, Ignace N. Structural and radiological parameters for the characterization of jawbone. *Clin Oral Implants Res.* 2006 Apr;17(2):124-33.
  25. Mavropoulos A, Kiliaridis S, Bresin A, Ammann P. Effect of different masticatory functional and mechanical demands on the structural adaptation of the mandibular alveolar bone in young growing rats. *Bone.* 2004 Jul;35(1):191-7.
  26. Majumdar S, Kothari M, Augat P, Newitt DC, Link TM, Lin JC, et al. High-resolution magnetic resonance imaging: three-dimensional trabecular bone architecture and biomechanical properties. *Bone.* 1998 May;22(5):445-54.
  27. Hsieh J, Molthen RC, Dawson CA, Johnson RH. An iterative approach to the beam hardening correction in cone beam CT. *Med Phys.* 2000 Jan;27(1):23-9.
  28. Verna C, Dalstra M, Lee TC, Melsen B. Microdamage in porcine alveolar bone due to functional and orthodontic loading. *Eur J Morphol.* 2005 Feb-Apr;42(1-2):3-11.
  29. Nevins ML, Camelo M, Rebaudi A, Lynch SE, Nevins M. Three-dimensional micro-computed tomographic evaluation of periodontal regeneration: a human report of intrabony defects treated with Bio-Oss collagen. *Int J Periodontics Restorative Dent.* 2005 Aug;25(4):365-73.
  30. Trisi P, Rebaudi A, Calvari F, Lazzara RJ. Sinus graft with biogran, autogenous bone, and PRP: a report of three cases with histology and micro-CT. *Int J Periodontics Restorative Dent.* 2006 Apr;26(2):113-25.